ECS Transactions, 103 (1) 1917-1925 (2021)
10.1149/10301.1917ecst ©The Electrochemical Society

Enhancing the Catalytic Activity of Lanthanum-Ceria Fluorite for Methane Conversion in SOFC

V. B. Vilela, V. V. Thyssen, L. N. Rodrigues, and F. C. Fonseca

Nuclear & Energy Research Institute, IPEN-CNEN/SP, University of São Paulo, São Paulo, Brazil

$A_2B_2O_7$ compounds with tailored compositions exhibit catalytic properties in a variety of high-temperature reactions, such as oxidative coupling of methane (OCM). $La_2Ce_2O_7$ performs well in OCM due to selective mobile oxygen species, and suitable alkaline sites. Doping with Ca^{2+} increases the alkalinity, which can considerably increase selectivity for C_2 products in OCM. We have explored the combustion synthesis to obtain homogeneous Ca^{2+}-doped $La_2Ce_2O_7$ materials to use as a catalytic layer in SOFC reactors for methane direct conversion to C_2. The addition of Ca^{2+} in the A site of $La_2Ce_2O_7$ resulted in the disordered fluorite-type crystalline structure. The formation of superficial oxygen vacancies related to the active oxygen species, which may benefit the OCM reaction, was detected. Electrochemical characterization showed no significant dependence of the conductivity with Ca^{2+}-doping.

Introduction

Methane conversion has been subject to extensive research for the past decades. However, most studies concern heterogeneous catalysis and considerably less attention was dedicated to both electrochemical and solid-state membrane reactors, such as solid oxide cell-type. The direct conversion of methane to higher hydrocarbons compounds (C_2) can take place by the oxidative coupling of methane (OCM – Reactions 1 and 2). (1-4)

$$2CH_4 + ½O_2 \leftrightarrows C_2H_6 + H_2O \quad [1]$$

$$2CH_4 + O_2 \leftrightarrows C_2H_4 + 2H_2O \quad [2]$$

Methane is a very stable molecule, and high temperatures are necessary for its conversion. The desired C_2 products (C_2H_6 and C_2H_4) are less stable than methane, thus, such high temperatures favor the complete oxidation to CO_x. In this context, using a solid-state membrane reactor, such as a solid oxide fuel cell (SOFC), to control the reacting species is an important advance to overcome some challenges of more standard fixed-bed reactors. A strategy that proved to result in better SOFC performance on OCM is using a proper catalytic layer to avoid reactions that lead to undesirable products, such as CO_2 and CO, and improve its stability. (1-4)

An effective catalyst for OCM must have electrophilic oxygen mobility and alkalinity on its surface. A typical $A_2B_2O_7$ compound that contains a trivalent rare earth metal at site A, such as lanthanum, can provide the necessary surface alkalinity for a good OCM catalyst.

Previous studies show that $La_2Ce_2O_7$ catalysts perform well in OCM, due to the selective mobile oxygen sites, suitable alkaline sites, and high thermal stability. The use of dopants, such as calcium, increases the material alkalinity, which can considerably increase selectivity for C_2 via the OCM process. Such materials can be obtained by the combustion method that can result in a favorable microstructure for a high-temperature catalyst. (5-7)

Combustion synthesis of materials has gained attention because it is a fast, economical, and energy-efficient process. Combustion synthesis methods can be categorized based on the physical nature of the reaction mixture itself, such as flame synthesis or gas-phase combustion, heterogeneous condensed phase combustion synthesis, and solution combustion synthesis (SCS). The SCS-based technique has been used to produce a wide variety of materials for different applications such as pigmentation, catalysis, electronic, magnetic materials, etc. Typically, SCS involves a self-sustaining reaction of a metal nitrate solution and an oxygen-containing fuel. The reaction between a fuel, oxygen, and species formed during nitrate decomposition provides conditions for the rapid spread of high temperature for the combustion reaction to occur. (8,9)

The present study aims to study single-phase Ca^{2+}-doped $La_2Ce_2O_7$ prepared by the combustion method, for the application as a catalytic layer at the anode of SOFC for the conversion of methane to C_2 by the oxidative coupling process.

Experimental

Preparation

The first step of the synthesis was stirring a solution with a small volume of water, $La(NO_3)_3.6H_2O$ (99.9 %, Sigma-Aldrich), $Ce(NO_3)_3.6H_2O$ (99.9 %, Sigma-Aldrich), and urea (CH_4N_2O, Nuclear) to obtain a gel of the precursor solution to $La_2Ce_2O_7$ (LCO) with 50:50 ratio of La^{3+} and Ce^{4+}. Nitrate salts were the oxidizer of the reaction and urea was used as fuel with two different proportions: stoichiometric and 150 % excess. The obtained gel was taken, in an alumina crucible, to a muffle at 500 ^oC to ignite the combustion reaction (Reaction 3), which was developed during ~ 4 min. The combusted material was then deagglomerated using an agate mortar to obtain the LCO sample powder (Fig. 1). For comparison, CeO_2 was also prepared using the same procedure.

$$2La(NO_3)_{3(s)} + 2Ce(NO_3)_{3(s)} + 10CH_4N_2O_{(s)} \rightarrow La_2Ce_2O_{7(s)} + 10CO_{2(g)} + 16N_{2(g)} + 20H_2O_{(g)} \quad [3]$$

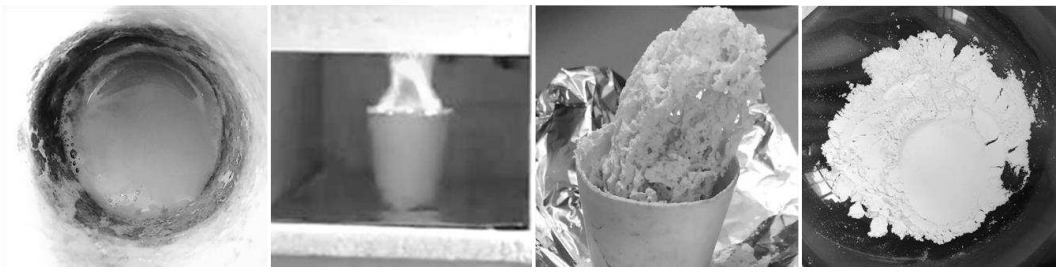

Figure 1. Combustion synthesis steps, from left to right: gel of the precursor solution, ignition process, combusted material, deagglomerated final powder.

For Ca^{2+}-doped samples, $La_{2-x}Ca_xCe_2O_7$ with x = 0.25 and 0.50 (Ca25-LCO and Ca50-LCO, respectively) compounds were produced following the same procedure adding $Ca(NO_3)_2.4H_2O$ (99 %, Sigma-Aldrich) in the precursor solution of the combustion process.

Characterization

X-ray diffraction (XRD) analysis of the synthesized materials was carried out in the Rigaku MiniFlex II with CuKα radiation. All crystalline phases were identified by Crystallograhica Search Match© software. Simultaneous thermogravimetric and differential thermal analysis (TG/DTA) of LCO powder were measured between room temperature and 1200 ºC under synthetic airflow (50 ml/min) with 10 ºC/min heating rate. Ca-LCO green cylindrical pellets with ~ 6 mm diameter were uniaxially pressed for dilatometry (TMA) analysis up to 1400 ºC in synthetic air flow with heating rate 10 ºC/min. Both TG/DTA and TMA analyses were performed using Setaram Labsys equipment. Raman spectra were measured using Horiba scientific MacroRaman with wavelength set at 785 nm. The microstructure of the as-prepared powders was analyzed by a scanning electron microscope (SEM) JEOL, JSM-6010LA. Ca-LCO pellets (10 mm diameter) were sintered at 1500 ºC for 2 h, with a heating rate of 10 ºC/min under air. Gold contact pads were painted with gold ink in the paralleled surface of the cylindrical pellets followed by curing under air at 800 ºC. The electrical properties of Ca-LCO sintered samples were studied by impedance spectroscopy (IS) under N_2 flow (20 ml/min) using a Novocontrol Alpha-A analyzer, in the 10 MHz to 1 Hz frequency range, with ac amplitude of 100 mV, in the 300-800 ºC temperature range.

Results and Discussion

The XRD patterns in Fig. 2a showed that the combustion synthesis with stoichiometric urea resulted in $La_2Ce_2O_7$ (LCO) as the main phase. However, additional peaks at 25.7º, 30.4º, 39.35º, and 43.65º (2θ) were detected and indexed as La_2O_3 (JCPDS #5-602) with the main diffraction peak at 30.35º. The La_2O_3 phase was observed on XRD after further heat treatments at 800 and 1100 ºC, suggesting heterogeneous combustion of the precursor during the synthesis. Therefore, a new synthesis with 150 % excess urea was carried out to ensure the complete reaction of all nitrates to obtain the single-phase LCO.

The excess urea LCO (JCPDS #04-12-6396) sample presented an XRD pattern similar to that of CeO_2 (Fig. 2b), with a displacement (see *inset* in Fig. 2b) of the main peak of diffraction to lower Bragg angle. The lower 2θ of LCO is consistent with the effective addition of La^{3+} into the CeO_2 structure because the La^{3+} ionic radius (1.16 Å) is larger than that of Ce^{4+} (0.97 Å). Moreover, the absence of additional diffraction peaks strongly suggests that single-phase LCO was formed during the combustion requiring no further heat treatment.

Much has been discussed about the crystalline structure of LCO samples and different symmetries have been proposed, such as pyrochlore-type structure or disordered fluorite. For the LCO samples synthesized in this study, we considered a fluorite-type crystalline structure, since the diffraction peaks referring to pyrochlore superstructure arrangement, located between 30º and 45º, were not detected. (11,12)

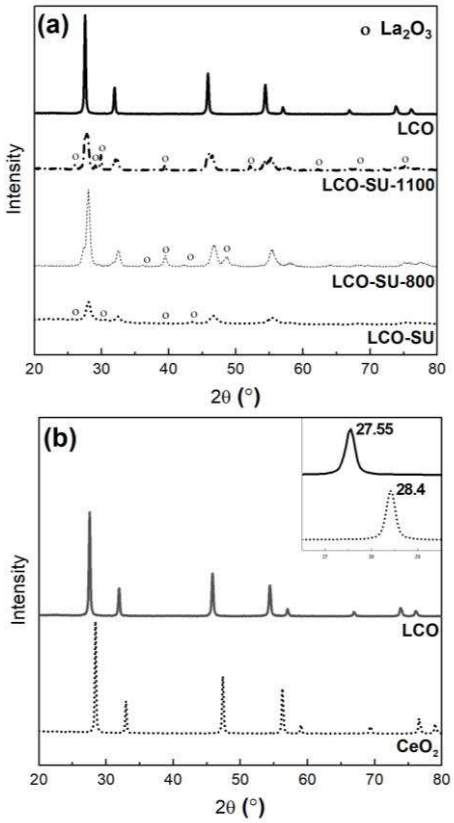

Figure 2. XRD patterns of (a) LCO obtained by stoichiometric urea combustion method: as-prepared (LCO-SU), after heat treatment at 800 ºC (LCO-SU-800), and at 1100 ºC (LCO-SU-1100); (b) LCO, and CeO_2 obtained by excess urea combustion method.

After obtaining the single-phase LCO, we incorporated different Ca^{2+} content substituting La^{3+} in the LCO structure. Solid-solution samples Ca-LCO presented a diffraction pattern similar to LCO (Fig. 3a), with the fluorite-type crystalline structure. The effective addition of Ca^{2+} into the LCO structure is indicated by the displacement of the main peak of diffraction to larger Bragg angles (Fig. 3b), as a result of the compression of the unit cell because the lower ionic radius of Ca^{2+} (1.12 Å) compared to that of La^{3+} (1.16 Å). (12-14)

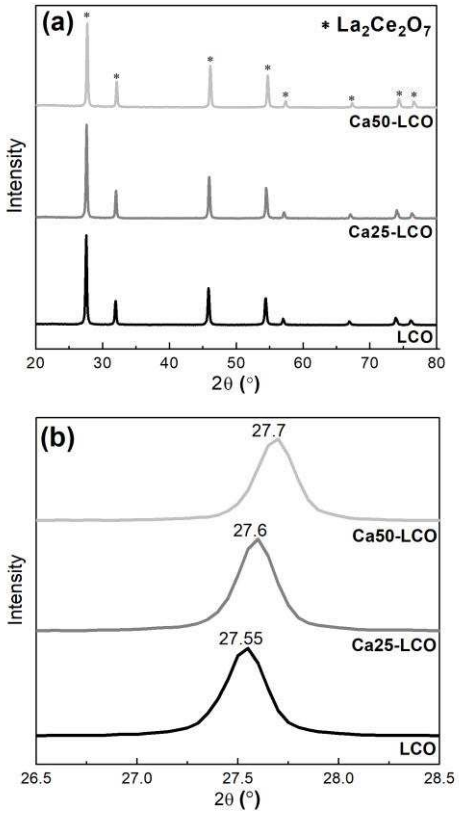

Figure 3. XRD patterns of (a) LCO and A site Ca-doped LCO obtained by excess urea combustion method, and (b) displacement with Ca^{2+} addition.

Raman spectroscopy (Fig. 4) was performed to identify the vibrational modes, oxygen vacancies formation, and the crystalline structure of the as-prepared solid solutions.

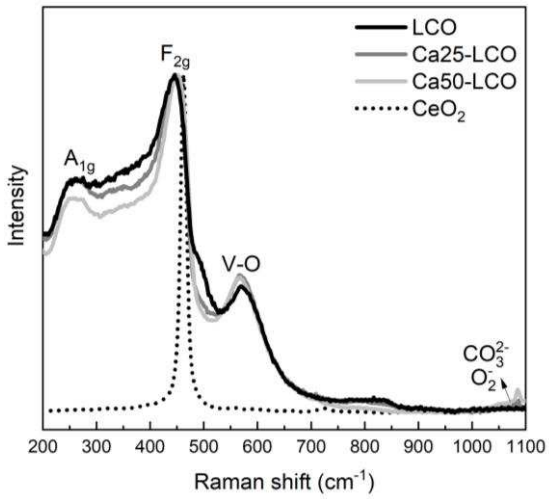

Figure 4. Raman spectroscopy for CeO_2, LCO, and Ca-doped LCO samples.

For LCO, the A_{1g} band, at 254 cm^{-1}, is associated with the formation of structure oxygen vacancies. The band at 448 cm^{-1} is attributed to the F_{2g} vibrational mode of fluorite structure, also present in CeO_2 spectra at 443 cm^{-1}, confirming the fluorite structure in agreement with XRD data. For pyrochlore-type structures the most significant band, expected at 300 cm^{-1} and associated with the B-O bond vibrations in E_g mode, is absent. The 567 cm^{-1} band

refers to the surface oxygen vacancies, which are generated by a random distribution of La^{3+} and Ce^{4+} in the crystal cell. An additional band related to surface oxygen vacancies is shown at 800 cm^{-1}. The formation of surface oxygen vacancies may benefit the dissociative adsorption of O_2 gaseous molecules in active electrophilic oxygen species on the surface of materials. Such oxygen species act as active sites for the OCM reaction, contributing to a more effective OCM catalyst. (12,13,15-17)

Raman spectra of Ca-LCO samples corroborate the results of XRD, confirming their fluorite structure. Along with LCO bands, Ca^{2+}-doped LCO samples exhibit peaks between 1050 and 1100 cm^{-1}, which has two main contributions: (i) the formation of the active surface oxygen species O_2^- (12,15); and (ii) the vibration of carbonate groups bonds, related to the reaction between surface calcium and atmosphere CO_2 (Reaction 4) (13,16,18):

$$CaO + CO_2 \leftrightarrows CaCO_3 \quad [4]$$

By comparing Raman spectra, it was observed a displacement of the band attributed to F_{2g} vibrational mode due to the doping process. This displacement depends on the ionic radius of the dopant, the larger the radius of the dopant the bigger is the displacement, by changing the Ce-O vibration frequency after the doping. (19)

Due to the characteristics of the combustion synthesis reaction, combining a fast temperature increase and the evolution of a large amount of gas-phase products, such method produces a unique surface morphology. As shown in SEM images (Fig. 5), as-prepared powders have a similar microstructure composed of porous sponge-like agglomerated particles with irregular shape. (20)

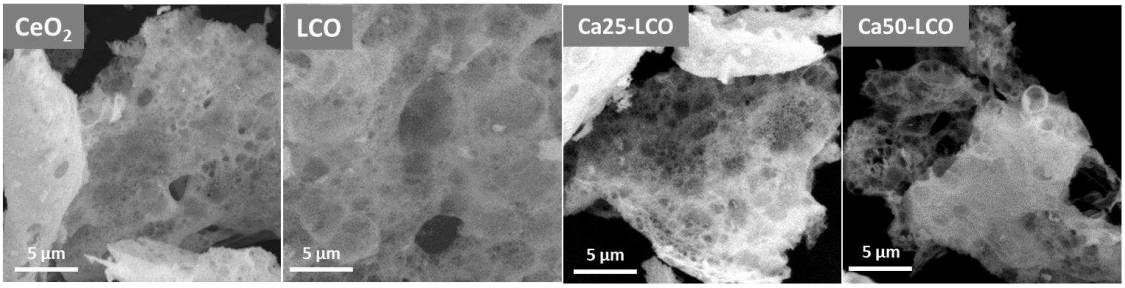

Figure 5. SEM images for ceria oxide, LCO, and A site Ca-doped LCO obtained by excess urea combustion method.

The thermal behavior of as-prepared LCO obtained by excess urea combustion method was investigated by TG/DTA as shown in Fig. 6a. The TG/DTA curves show that there is no significant weight loss of the LCO. The approximate mass loss of 2 % of the initial weight may be the loss of surface water and confirms excellent thermal stability for LCO synthesized by excess urea combustion method.

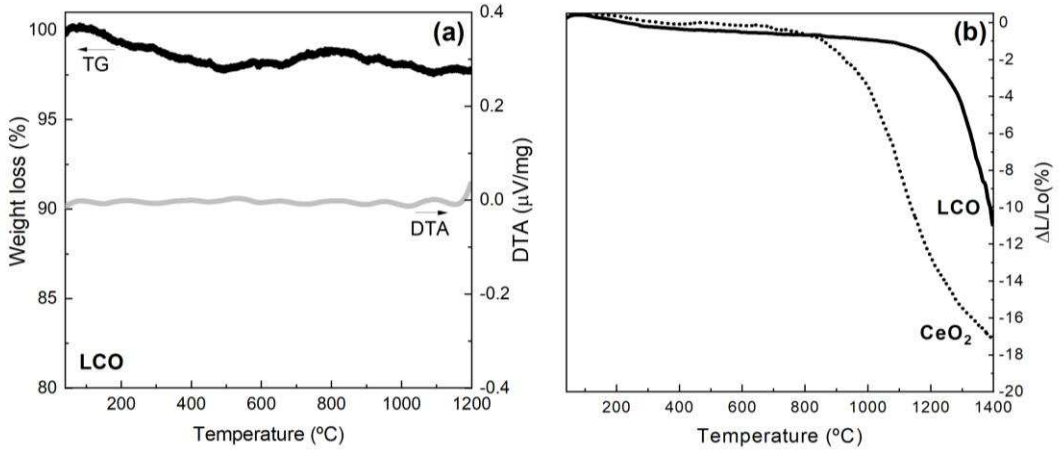

Figure 6. (a) TG/DTA analysis of as-prepared LCO obtained by excess urea combustion method, and (b) Dilatometric measurements of LCO and CeO_2 obtained using excess urea.

Dilatometry analysis of CeO_2 and LCO was carried out to study the densification process (Fig. 6b). The LCO had a relative green density of 42 % of the theoretical density and the final relative density after dilatometry was 56 %. For CeO_2 the green and after dilatometry density values were 40.7 % and 69 %, respectively. The addition of La^{3+} into the CeO_2 structure changed the sintering behavior of CeO_2 by increasing the onset shrinkage temperature and decreasing the total retraction. None of the samples reached the final sintering stage at 1400 ºC. Pellets of the single-phase LCO, Ca25-LCO, and Ca50-LCO materials were then sintered at 1500 ºC for 2 h for electrical characterization.

The electrical properties were studied by impedance spectroscopy (IS) measurements under inert atmosphere (N_2), as shown in Fig. 7a. The IS data showed that both LCO and Ca^{2+}-doped samples exhibited one semicircle arc in the high frequency region (1 MHz) and a low frequency contribution, likely related to electrode reactions (Fig. 7a).

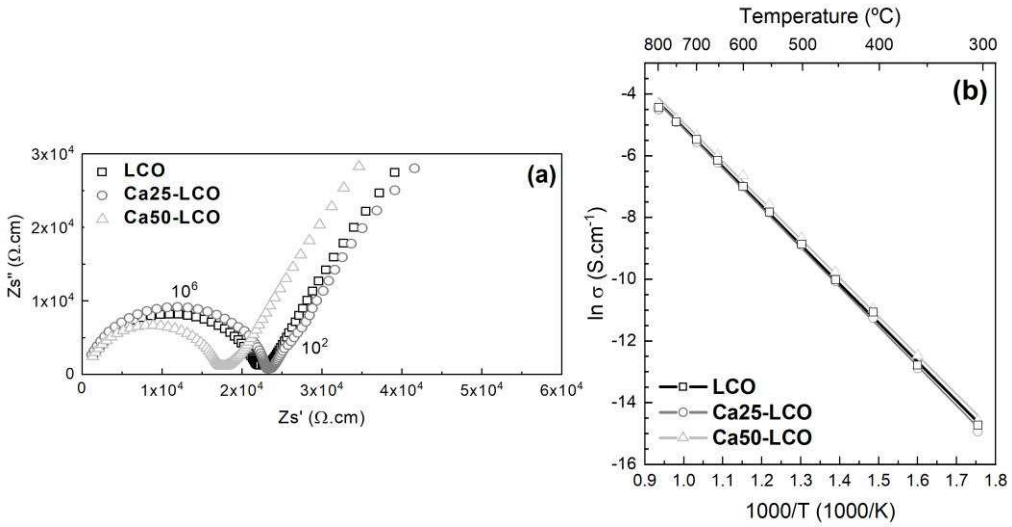

Figure 7. (a) Nyquist plots measured at 450 ºC in N_2 and (b) Arrhenius plots for A site Ca-doped LCO obtained by excess urea combustion method.

Arrhenius plots of total conductivity extracted from the impedance arc at high frequency are shown in Fig. 7b. Using the Arrhenius equation (19), the activation energy

was calculated in the temperature range 300-800 °C. The calculated activation energy values are similar for all samples, ~ 1.10 eV, and consistent with the typical values of ceria-lanthanum system oxygen ion conductors previous reported (17,22-24). The ionic conductivity can be enhanced in rare-earth doped-ceria ceramics by the increase of oxygen vacancy (21). However, no significant dependence of the conductivity was observed with Ca^{2+}-doping.

Conclusion

The results showed that LCO material was successfully synthesized by the combustion method by adding excess urea, and a single-phase Ca^{2+}-doped LCO with fluorite-type crystalline structure was obtained.

The calcium addition on the A-site of the LCO fluorite structure resulted in oxygen vacancies and carbonate species, as inferred from Raman spectroscopy data. Impedance data showed no significant change of the conductivity. Further measurements are underway to study the conductivity and catalytic properties towards OCM reaction of the LCO phase.

Acknowledgments

We are thankful for the Energy & Nuclear Research Institute (IPEN-CNEN/SP) infrastructure. Thanks are also due to the Center for Innovation on New Energies CINE-Shell/ANP- FAPESP (2017/11937-4) financial support. F. C. Fonseca is a CNPq fellow.

References

1. S. Majhi, P. Mohanty, H. Wang, and K. K. Pant, *J. Energy Chem.*, **22**, 543 (2013).
2. Y. Gambo, S. Jalil, S. Triwahyono, and A. A. Abdulrasheed, *J. Ind. Eng. Chem.*, **59**, 218 (2018).
3. S. Liu, X. Tan, K. Li, and R. Hughes, *Catal. Rev. Sci. Eng.*, **43**, 147 (2001).
4. A. Cruellas, T. Melchiori, F. Gallucci, and M. van Sint Annaland, *Energy Technol.*, **8**(8), 1900148 (2019).
5. E. V. Kondratenko, T. Peppel, D. Seeburg, V. A. Kondratenko, N. Kalevaru, A. Martin, and S. Wohlrab, *Catal. Sci. Technol.*, **7**(2), 366 (2016).
6. U. Zavyalova, M. Holena, R. Schlçgl, and M. Baerns, *ChemCatChem*, **3**(12), 1935 (2011).
7. V. Esposito and E. Traversa, *J. Am. Ceram. Soc.*, **91**, 1037 (2008).
8. A. S. Mukasyan, P. Epstein, and P. Dinka, *Proc. Combust. Inst.*, **31**, 1789 (2007).
9. W. Wen and J. M. Wu, *RSC Adv.*, **4**, 58090 (2014).
10. E. R. Andrievskaya, O. A. Kornienko, A. V. Sameljuk, and A. Sayir, *J. Eur. Ceram. Soc.*, **31**(7), 1277 (2011).
11. S. Shi, Y. Yang, P. Guo, J. Wang, L. Geng, and L. Fu, *J. Lumin.*, **206**, 91 (2018).
12. J. Zamudio-García, J. M. Porras-Vázquez, J. Canales-Vázquez, A. Cabeza, E. R. Losilla, and D. Marrero-López, *Inorg. Chem.*, **58**(14), 9368 (2019).
13. J. Xu, Y. Zhang, Y. Liu, X. Fang, X. Xu, W. Liu, R. Zheng, and X. Wang, *Eur. J. Inorg. Chem.*, **2019**(2), 183 (2019).

14. Z. Hong-Song, W. Yuan, L. Gang, C. Xiao-Ge, and W. Xin-Li, *J. Alloy Compd.*, **537**, 141 (2012).
15. J. Xu, Y. Zhang, X. Xu, X. Fang, R. Xi, Y. Liu, R. Zheng, and X. Wang, *ACS Catal.*, **9**, 4030 (2019).
16. Y. Zhang, J. Xu, X. Xu, R. Xi, Y. Liu, X. Fang, and X. Wang, *Catal. Today*, **355**, 518 (2019).
17. T. Tu, B. Zhang, J. Liu, K. Wu, and K. Peng, *Electrochim. Acta*, **283**, 1366 (2018).
18. V. V. Thyssen and E. M. Assaf, *Fuel*, **254**, 115592 (2019).
19. K. C. Anjaneya, G. P. Nayaka, J. Manjanna, G. Govindaraj, and K. N. Ganesha, *J. Alloy Compd.*, **585**, 594 (2014).
20. A. Kumar, A. S. Mukasyan, and E. E. Wolf, *Appl. Catal. A-Gen.*, **401**, 20 (2011).
21. C. Tian and S-W. Chan, *Solid State Ion.*, **134**, 89 (2000).
22. J. Zamudio-García, L. dos Santos-Gómez, J. M. Porras-Vázquez, E. R. Losilla, and D. Marrero-López, *J. Alloy Compd.*, **816**, 152600 (2020).
23. B. Zhang, Z. Zhong, T. Tu, K. Wu, and K. Peng, *J. Power Sources*, **412**, 631 (2019).
24. H. Yamamura, H. Nishino, K. Kakinuma, and K. Nomura, *J. Ceram. Soc. Jpn.*, **111**(12), 902 (2003).